

Provided for non-commercial research and education use.
Not for reproduction, distribution or commercial use.



This article appeared in a journal published by Elsevier. The attached copy is furnished to the author for internal non-commercial research and education use, including for instruction at the authors institution and sharing with colleagues.

Other uses, including reproduction and distribution, or selling or licensing copies, or posting to personal, institutional or third party websites are prohibited.

In most cases authors are permitted to post their version of the article (e.g. in Word or Tex form) to their personal website or institutional repository. Authors requiring further information regarding Elsevier's archiving and manuscript policies are encouraged to visit:

<http://www.elsevier.com/copyright>



Influence of local and external processes on the annual nitrogen cycle and primary productivity on Georges Bank: A 3-D biological–physical modeling study

Rubao Ji^{a,*}, Cabell Davis^a, Changsheng Chen^b, Robert Beardsley^c

^a Department of Biology, Woods Hole Oceanographic Institution, Woods Hole, MA 02543, United States

^b The School for Marine Science and Technology, University of Massachusetts Dartmouth, New Bedford, MA 02744, United States

^c Department of Physical Oceanography, Woods Hole Oceanographic Institution, Woods Hole, MA 02543, United States

Received 7 March 2007; received in revised form 10 August 2007; accepted 19 August 2007

Available online 8 September 2007

Abstract

Georges Bank is one of the world's most highly productive marine areas, but the mechanisms of nutrient supply to support such high productivity remain poorly understood. Intrusions of nutrient-poor Labrador Slope Water (LSW) into the Gulf of Maine (NAO-dependent) potentially can reduce nutrient delivery to the bank, but this mechanism has not been quantitatively examined. In this paper, we present the first whole-year continuous model simulation results using a biological–physical model developed for the Gulf of Maine/Georges Bank region. This high-resolution three-dimensional coupled model consists of the Finite Volume Coastal Ocean Model (FVCOM) and a Nitrogen–Phytoplankton–Zooplankton–Detritus (NPZD) model, and was used to examine the influences of local and external processes on nitrogen and phytoplankton dynamics on Georges Bank. The model captured the general pattern of spatial-temporal distributions of nitrogen and phytoplankton and provided a diagnostic analysis of different processes that control nitrogen fluxes on Georges Bank. Specifically, numerical experiments were conducted to examine seasonal variation in nitrogen transport into the central bank (new nitrogen supply) versus nitrogen regenerated internally in this region. Compared with previous observation-based studies, the model provided a quantitative estimate of nitrogen flux by integrating the transport over a longer time period and a complete spatial domain. The results suggest that, during summer months, internal nitrogen regeneration is the major nitrogen source for primary production on the central bank, while nitrogen supply through physical transport (e.g. tidal pumping) contributes about 1/5 of the total nitrogen demand, with an estimated on-bank nitrogen transport at least 50% less than previous estimates. By comparing the model runs using different nitrogen concentrations in deep Slope Water, the potential influence of NAO-dependent intrusions of LSW was examined. The results suggest that the change of nitrogen concentration in the deep Slope Water may not have a significant impact on nitrogen and phytoplankton dynamics on the well-mixed central bank, largely due to limited nutrient exchange across the tidal mixing front and enhanced near-frontal nutrient uptake. However, relatively more significant impact was observed in the model simulations if both well-mixed and seasonally-stratified areas (inside 100 m isobath of the bank) were considered in flux calculations.

© 2007 Elsevier B.V. All rights reserved.

Keywords: Nitrogen cycle; Phytoplankton productivity; Modeling; Biological-physical coupling

* Corresponding author. Tel.: +1 508 289 2986.

E-mail address: rji@whoi.edu (R. Ji).

1. Introduction

Georges Bank (GB), a shallow submarine bank located in the south of the Gulf of Maine (GoM) (Fig. 1), has long been recognized as one of the world's most biologically productive areas. Annual primary productivity in the tidally mixed shallow area of the bank (455 gC m^{-2}) is about three times the mean for world continental shelves (O'Reilly et al., 1987). Numerous studies have been conducted to understand why the GB system is so productive at the lower trophic level (Cura et al., 1987; Klein et al., 1987; O'Reilly et al., 1987; Walsh et al., 1987; Horne et al., 1989; Townsend and Pettigrew, 1997). Yet the mechanism of nutrient supply to support such high

productivity remains as an “unsolved mystery” (Brink, 2004). Since nitrogen-fixation is not significant in these systems (Vitousek and Howarth, 1991), new nitrogen is typically supplied to shelf ecosystems through wind or tidally driven upwelling and/or by terrestrially-derived (usually nutrient-enriched) freshwater discharge. It is believed that terrestrial nutrient sources are not important on GB because the system is far from land, providing an opportunity to examine processes controlling input of deep off-bank nutrients into the GB system.

A straightforward way to identify the nitrogen source is to examine the internal nitrogen cycling (by biological processes) and the external transport from the surrounding areas (through physical processes). Most previous studies

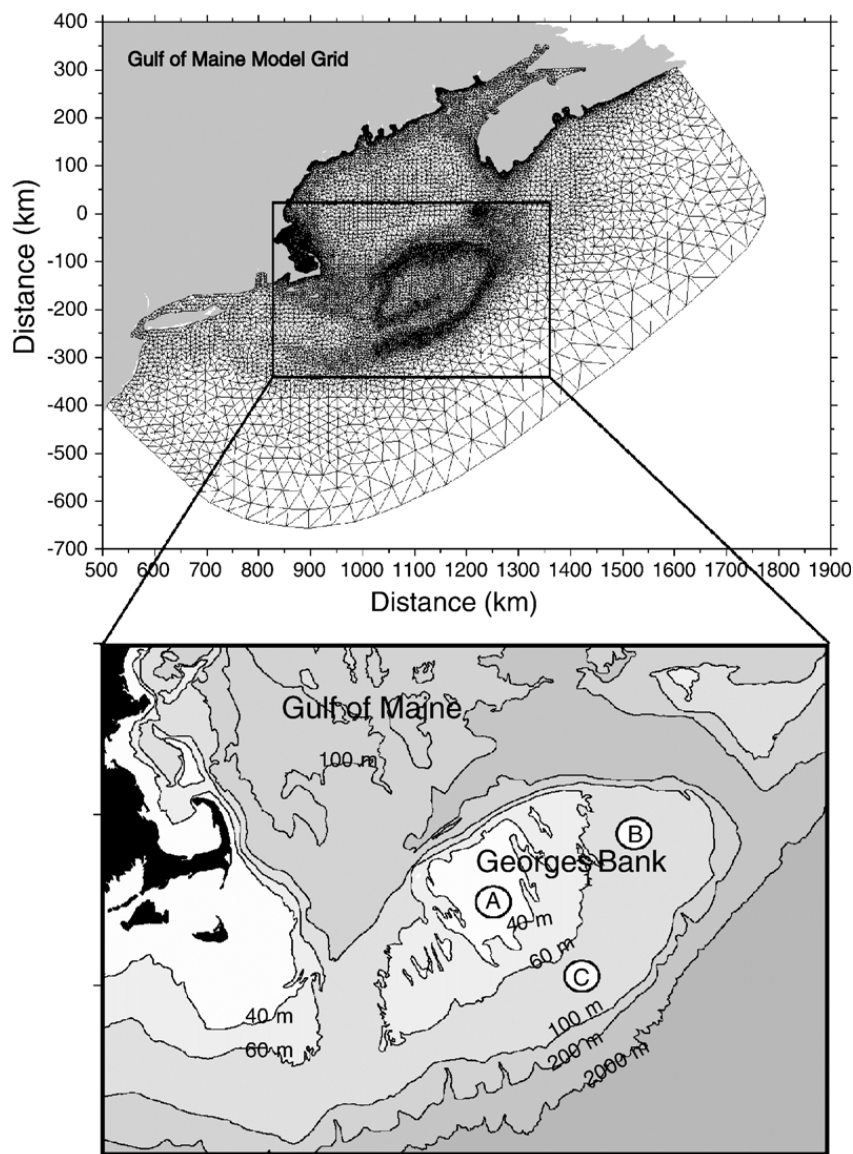


Fig. 1. Model grids for GoM/GB FVCOM (top panel) and bathymetry of Georges Bank (bottom panel). The labels A, B and C are locations for data-model comparisons described later.

of GB, including field measurements (e.g. Loder and Platt, 1985; Horne et al., 1989, 1996; Townsend and Pettigrew, 1997) and process-oriented modeling (e.g. Franks and Chen, 1996), have focused on nitrogen dynamics during summer when nutrients on the well-mixed central bank are nearly depleted (Pastuszak et al., 1982; Walsh et al., 1987). All these studies have converged to a similar conclusion: internal nitrogen recycling plays a dominant role in sustaining the observed high primary productivity on central GB in summer. There is, however, noticeable divergence among different studies in quantifying the relative contribution of physical nitrogen transport across the tidal mixing front located near the 60-m isobath around the bank. For instance, Horne et al. (1989) estimated $\sim 5 \times 10^3 \text{ mol N s}^{-1}$ for the total cross-frontal nitrogen flux, which is an order of magnitude greater than the flux estimated by Townsend and Pettigrew (1997). Low temporal and spatial resolution in the field measurements are likely the major reasons for such a large discrepancy. In a dynamic system like GB, where biological and physical processes interact with strong nonlinearity and are influenced by varying local and external forcings, the flux estimation based on short-term (days) measurements in a few stations will inevitably have large uncertainties.

In addition to the extensive studies on the summer-time nitrogen dynamics described above, a considerable amount of work has been conducted to understand the winter-spring nitrogen and plankton cycles on GB (Townsend and Thomas, 2001, 2002; Ji et al., 2006a,b) as a part of the on-going GLOBEC (Global Ocean Ecosystem Dynamics) GB Program (GLOBEC, 1992; Wiebe et al., 2002). However, due to the limitations in the temporal and spatial coverage of the observations and models and due to the lack of measurements in biological rates rather than the standing stocks, many important questions remain to be answered, including: (1) What is the annual cycle of nitrogen flux contributed by internal biological recycling versus physical transport processes? (2) When does the system shift from a new production dominated to a recycled-production dominated system? (3) When and how is nitrogen in the system being recharged? and (4) What is the potential influence on biological productivity of large-scale external forcing, such as the NAO-induced change between Warm Slope Water (WSW) and Labrador Slope Water (LSW) inflows that have different nitrogen concentrations (Townsend et al., 2006).

In this paper, we describe the results of a biological–physical model used to address the above questions. With the help of field measurements for calibration and validation, the model served as a unique tool for

quantifying the complex dynamical interactions between the local biological and physical processes and influences of external forcings. This modeling approach allowed us to integrate and distinguish different nitrogen flux quantities at different temporal and spatial scales, thus overcoming limitations of the observational coverage. The model described here is the first 3-D biological–physical model that incorporates realistic topography and surface/open boundary conditions and run continuously throughout the year in the GoM/GB region. With this model, we were able to better quantify daily to seasonal and local to bank-wide nitrogen fluxes. Here we present only the model results for year 1995 (chosen from five-year simulations from 1995 to 1999) as a case study, given that the general pattern of seasonal nitrogen/phytoplankton dynamics and nitrogen flux is similar in different years.

2. Methodology

The coupled model system includes a hydrodynamics model, the Finite Volume Coastal Ocean Model (FVCOM), and a four-compartment (nitrogen–phytoplankton–zooplankton–detritus, NPZD) biological model. The following is a detailed description of the two models.

2.1. Hydrodynamics model

FVCOM is a prognostic, unstructured grid, finite-volume, free-surface, 3-D primitive equation coastal ocean circulation model (Chen et al., 2003a, 2006a,c). In common with other coastal models, FVCOM uses the modified Mellor and Yamada level 2.5 (MY-2.5) and Smagorinsky turbulent closure schemes for vertical and horizontal mixing, respectively (Smagorinsky, 1963; Mellor and Yamada, 1982; Galperin et al., 1988), and a generalized terrain-following coordinate to match bottom topography. FVCOM is solved numerically by flux calculation using the integral form of the governing equations over an unstructured triangular grid. This approach combines the best features of finite-element methods (grid flexibility) and finite-difference methods (numerical efficiency and code simplicity) and provides a more accurate numerical representation of momentum, mass, salt, heat, and tracer conservation than other coastal ocean models (Chen et al., 2007). The ability of FVCOM to accurately solve scalar conservation equations, in addition to the topological flexibility provided by unstructured meshes and the simplicity of the coding structure, makes FVCOM ideally suited for interdisciplinary applications in coastal waters (Chen et al., 2006a; Ji et al., 2006a,c).

The model domain covers the GoM/GB and is enclosed by an open boundary running from the Nova Scotian shelf west of the Laurentian Channel down to the New Jersey shelf (Fig. 1). The horizontal resolution of the unstructured model grid is ~ 1 km near the coast and around the 60-m and 200-m isobaths on GB, and about 5–8 km in the interior of the GOM and near the open boundary. In the vertical, a uniform σ coordinate grid is used, with a vertical resolution of $\Delta\sigma=0.0323$ (31 points in the vertical). This resolution corresponds to ~ 1.3 –6.7 m vertical resolution over the depth range of 40–200 m on GB and 10-m spacing over the off-bank depths of 300 m (the model has a cut-off depth of 300 m in slope region). The time steps for the external and internal modes are 12 and 120 s, respectively. The model was initialized with homogeneous temperature (T) and salinity (S) fields on December 1, 1994 and integrated in time to December 15, 1994 with realistic tidal forcing (including the five major components, M_2 , S_2 , N_2 , O_1 and K_1) specified along the open boundary. The initial condition of the flow field at each grid point was specified using the Foreman tidal forecast program built on the FVCOM tidal model output. The purpose of running the model under these homogeneous conditions is to spin up the tidal component. The model then was restarted from December 15, 1994 with the “hot-start” initial condition of T and S specified using December climatology fields and continued numerical integration until December 31, 1994 to spin up the baroclinic circulation driven by stratified tidal rectification and buoyancy forcing. The real-time wind stress, heat flux, river discharge, and upstream inflow condition were added starting on January 1, 1995 and numerical integration continued until the end of 1995. The surface meteorological forcings (wind stress and heat flux) were derived from the fifth-generation mesoscale regional weather model (MM5), which was originally developed by NCAR/Penn State (Dudhia et al., 2003) and has been configured to model the GoM/GB region in hindcast and forecast modes (Chen et al., 2005).

2.2. Biological model

The schematic of the NPZD model is shown in Fig. 2. Nitrogen is considered as the only limiting nutrient,¹ and this element is used as a tracer for biological variables.

¹ Silicate is another possible limiting nutrient during early spring (Townsend and Thomas, 2001, 2002). The complex role of silicate in the food web and its relationship with nitrogen were discussed in Ji et al. (2006b).

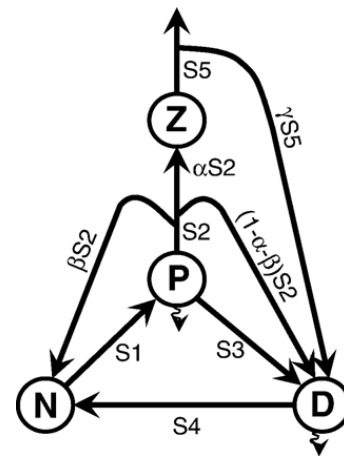


Fig. 2. Structure of the nitrogen–phytoplankton–zooplankton–detritus (NPZD) model.

Many key aspects of lower trophic level food web dynamics are described in this model using methods that are widely accepted in the marine ecosystem modeling community, including (1) Michaelis–Menten kinetics in nutrient uptake, (2) Holling type II functional response of zooplankton grazing on phytoplankton, (3) temperature/light-dependent growth for phytoplankton and temperature-dependent grazing and respiration for zooplankton, (4) self-shading of phytoplankton growth, and (5) sinking of phytoplankton and detritus. Compared to the classic NPZ model (Franks et al., 1986), the addition of the detritus compartment allows for the inclusion of remineralization, particles sinking out of the surface mixing layer, and grazing of zooplankton on detritus. Simple NPZD-type models have proven to be useful in capturing bulk ecosystem properties and dynamics (e.g. Friedrichs and Hofmann, 2001; Franks, 2002; Olascoaga et al., 2005), given that more complex models (compared to simple NPZD model) are often fraught with difficulties, including poorly understood ecology, lack of data, and parameterization problems (e.g. Anderson, 2005, 2006) and adding more complexity into the model might not be advantageous (e.g. Friedrichs et al., 2006). In addition, the dynamics of the NPZD model have been examined analytically using different model configurations and parameters in cases of no physical forcing (Edwards, 2001) and with simple forcings (Popova et al., 1997). These studies provide a solid foundation for this NPZD model to be coupled with a 3-D physical model and for examining its behavior under much more complex forcings.

Symbols S1–S5 are used to represent different processes in controlling the source and sink terms of the biological state variables (S1: nitrogen uptake by

phytoplankton; S2: zooplankton grazing on phytoplankton; S3: phytoplankton mortality; S4: remineralization of detritus; S5: zooplankton mortality). These terms can be described as:

$$S1 = \mu_{\max} f(I) f(N) P$$

$$= \mu_{\max} \frac{N}{K_N + N} \left[(1 - e^{-\hat{\alpha} I}) e^{-\hat{\beta} I} \right] P \quad (1)$$

$$S2 = g_{\max} f(P) Z = g_{\max} \frac{P^2}{(K_p)^2 + P^2} Z; \quad (2)$$

$$S3 = \lambda P; \quad (3)$$

$$S4 = \varepsilon D; \quad (4)$$

$$S5 = m Z^2. \quad (5)$$

where N , P , Z and D represent nitrogen, phytoplankton, zooplankton and detritus, respectively. Notice that zooplankton mortality has a quadratic form (as opposed to linear form for phytoplankton), a commonly-used treatment for NPZD-type model following [Steele and Henderson \(1992\)](#). The definitions and values of all the

parameters are listed in [Table 1](#). The change of biological quantities over time (without considering the advection, diffusion and sinking) then can be described as:

$$\frac{dN}{dt} = -S1 + \beta S2 + S4; \quad (6)$$

$$\frac{dP}{dt} = S1 - S2 - S3; \quad (7)$$

$$\frac{dZ}{dt} = \alpha S2 - S5; \quad (8)$$

$$\frac{dD}{dt} = (1 - \alpha - \beta) S2 + S3 + \gamma S5 - S4. \quad (9)$$

For all the source and sink terms, the temperature effects are incorporated as a simple Q_{10} relationship in the form of $S = S_b (Q_{10})^{(T - T_b) / 10}$, with S and S_b representing the biological rates at the instantaneous temperature (T) and the base temperature (T_b , set to 10 °C), respectively.

The intensity of photosynthesis active radiation (PAR) at each depth is a function of the surface PAR

Table 1
Definitions and values of the parameters used in the biological model

Symbol	Code	Definition	Value	Unit
μ_{\max}	r_pumax	Maximum phytoplankton growth rate ($T=10$ °C)	1.5	day ⁻¹
λ	r_ploss	Phytoplankton mortality ($T=10$ °C)	0.1	day ⁻¹
g_{\max}	r_zgmax	Maximum grazing rate of zooplankton on phytoplankton ($T=10$ °C)	0.3	day ⁻¹
m	r_zmort	Zooplankton density dependent mortality rate ($T=10$ °C)	0.2	($\mu\text{M N}$) ⁻¹ day ⁻¹
ε	r_dremi	Detritus remineralization rate ($T=10$ °C)	0.1	day ⁻¹
α	c_alpha	Zooplankton assimilation coefficient	0.3	Dimensionless
β	c_beta	Zooplankton excretion coefficient	0.3	Dimensionless
γ	c_gama	Recycle coefficient of zooplankton loss term	0.7	Dimensionless
$\hat{\alpha}$	alphax	Initial slope of the P–I curve normalized to μ_{\max}	0.025	(W m ⁻²) ⁻¹
$\hat{\beta}$	betax	Light inhibition coefficient	0.001	(W m ⁻²) ⁻¹
K_N	Knn	Half saturation constant of phytoplankton uptake on nitrogen	1.0	$\mu\text{M N}$
K_P	kpp	Half saturation constant of zooplankton grazing on phytoplankton	0.3	$\mu\text{M N}$
a_W	attw	Light attenuation coefficient by pure water	0.1	m ⁻¹
a_P	attp	Light attenuation coefficient by phytoplankton	0.04	m ⁻¹ ($\mu\text{M N}$) ⁻¹
a_D	attd	Light attenuation coefficient by detritus	0.04	m ⁻¹ ($\mu\text{M N}$) ⁻¹
w_P	wskp	Phytoplankton sinking velocity	1.0	m day ⁻¹
w_D	wskd	Detritus sinking velocity	10.0	m day ⁻¹
Q_{10}	q10	Temperature coefficient	2.0	Dimensionless
θ	parfr	Ratio of PAR (photosynthesis active radiation) versus surface shortwave radiation	0.43	Dimensionless

and the light attenuation profile (including self-shading), and is described as the following equation:

$$I(z) = I_0 \exp\left(-a_W z - a_P \int_{-z}^0 P dz - a_D \int_{-z}^0 D dz\right). \quad (10)$$

where $I(z)$ is PAR at depth z ; I_0 is surface irradiance; and a_W , a_P and a_D are light attenuation coefficients for pure water, phytoplankton and detritus, respectively. In the numerical model, the thickness of each vertical layer can be >10 m in deep areas. Therefore, an average value of irradiance for each layer needs to be computed. Let I_s and I_b denote PAR at the surface and the bottom of layer k , respectively, and let D_k denote the thickness of layer k and z_k the depth below the surface of layer k , then the average PAR in the layer k , (\bar{I}_k), is

$$\begin{aligned} \bar{I}_k &= \frac{1}{D_k} \int_0^{D_k} I(z_k) dz_k \\ &= \frac{1}{D_k} \int_0^{D_k} I_s \exp(-\varphi(k)z_k) dz_k = \frac{(I_s - I_b)}{D_k \varphi(k)}. \end{aligned} \quad (11)$$

where $\varphi(k)$ is the light attenuation coefficient in layer k , and computed as a function of concentrations of phytoplankton ($P(k)$) and detritus ($D(k)$) in layer k :

$$\varphi(k) = a_W + a_P P(k) + a_D D(k). \quad (12)$$

For phytoplankton and detritus, the sinking terms, $-w_P \frac{\partial P}{\partial z}$ and $-w_D \frac{\partial D}{\partial z}$, were added into Eqs. (7) and (9), respectively.

2.3. Numerical experiment

For the baseline model run (control case), the initial distribution of nitrogen and phytoplankton were specified using the climatology condition in December derived from the data compiled for the entire GoM/GB region since 1931, with about 18,023 and 32,997 total data points for nitrate and chlorophyll concentrations, respectively. The data sources include (1) BIO-MEDS (Bedford Institute of Oceanography — Marine Environmental Data Service); (2) MARMAP (Marine Monitoring Assessment and Prediction) and subsequent ECOMON (Ecological Monitoring); and (3) GLOBEC. Due to the lack of data on total zooplankton and detritus distribution, their initial concentrations were assumed to be homogeneous both horizontally and vertically, with

values of 0.1 and 1.0 $\mu\text{M N}$ for zooplankton and detritus, respectively. To test the effect of initial condition on model behaviors (e.g. time scale to reach dynamic equilibrium), trial model runs with varying initial concentration of biological variables were conducted and the results indicated that the memory of initial condition is less than a month in most cases.

To examine the possible impact of deep nutrient variability on the fluxes and seasonal cycles of nitrogen and phytoplankton (experimental case), the model was run with increased nitrogen concentrations in water deeper than 100 m, while keeping the same initial distributions for the other biological variables. Specifically, the nitrogen concentration below 100 m was set to be 50% higher than the climatology condition at each depth. This case is referred as the “bottom-enhanced condition” (BEC) case in the later text, as opposed to the “baseline” case where nitrogen was initialized with climatology conditions throughout the model domain. This examination of deep nutrient variability is used to gain insight into the potential impact of NAO-induced variation in deep Slope Water nutrient concentration on biological productivity on GB (Townsend et al., 2006).

3. Results and discussion

3.1. Physical fields

The GoM/GB FVCOM model system has been used to make a continuous hindcast simulation from 1995 to 2006. Comparisons of the model results with tides, in-situ T/S and current data show in general good agreement and small data-model misfits (Chen et al., 2006b; Cowles et al., submitted for publication). The detailed hydrodynamics model results, including monthly and daily averaged model results (T/S and residual currents), can be found on the world-wide web at the address http://fvcom.smast.umassd.edu/research_projects/GB/. The model tides are in good agreement with available surface elevation and current data, with overall uncertainties for the dominant M2 component of less than 3 cm in amplitude, 5° in phase, and 3 cm s⁻¹ in the tidal current major axis (Chen et al., 2006b). The modeled sub-tidal currents and stratification also agree well with existing in-situ measurements, capturing the seasonal cycle in vertical stratification and associated variation in strength of the around-bank circulation on GB. In addition, the model captures the interannual variability of temperature/salinity in the GoM through adjustment of the upstream T/S boundary conditions on the Scotian shelf and along the slope.

The circulation patterns and frontal dynamics on GB have been documented in previous observational and modeling studies, including the clockwise residual circulation around the bank (Loder, 1980; Butman et al., 1982; Chen et al., 1995; Limeburner and Beardsley, 1996), seasonal tidal mixing front around the shallow cap of the bank (~40 m isobath on the northern flank and 50–60 m isobaths along the southern flank) (Flagg et al., 1987; Chen et al., 1995), and the permanent shelf-break front along the outer edge of the southern flank (~80–200 m isobaths) (Flagg et al., 1987). These hydrodynamic features have been captured in this model. The clockwise residual circulation around the bank can be seen clearly in both winter (Fig. 3, top panel) and summer (Fig. 3, bottom panel), with the maximum velocity reaching ~30 cm s⁻¹ on the northern flank. The circulation around the bank, especially the jet currents near the tidal mixing front and the shelf-break front are intensified during the summer season, largely due to the establishment of geostrophic flow associated with seasonal heating and the tidal mixing front during this time of the year (Chen et al., 1995, 2001). The general pattern of clockwise circulation persists throughout the year as seen from the model results animations (see above mentioned website). The location of the fronts can be seen more clearly from the

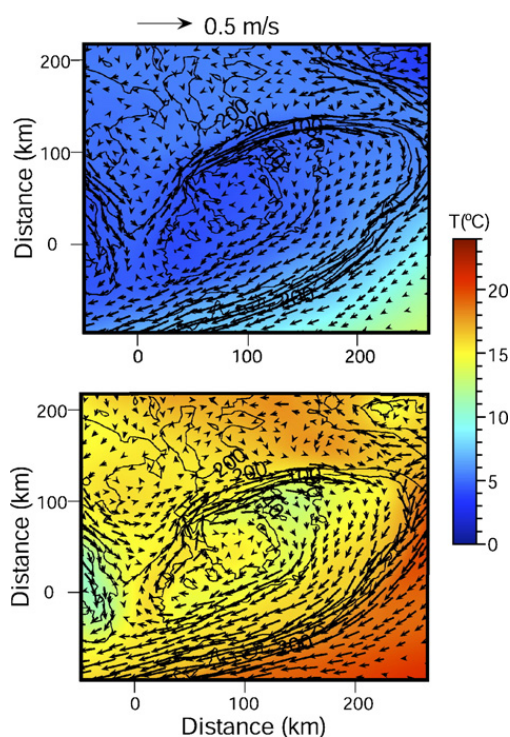


Fig. 3. Model distributions of surface temperature (colored contour) and sub-tidal currents (arrows) in March (top panel) and August (bottom panel), 1995. Notice that the vectors have been sub-sampled from the original high-resolution model grid for clarity.

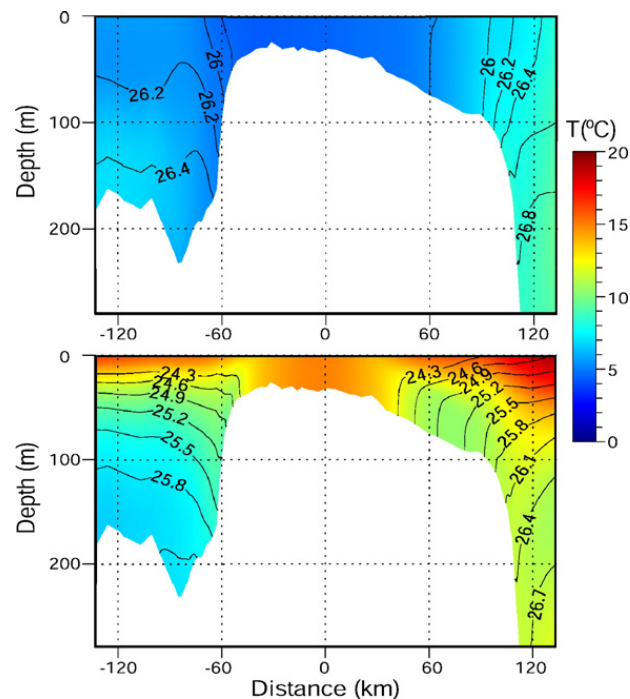


Fig. 4. Model distributions of temperature (colored contour) and sigma-t (labeled contour) along a transect across Georges Bank in March (top panel) and August (bottom panel), 1995. Location of transect line is shown in Fig. 5.

transect views of temperature and sigma-t distributions (Fig. 4). It can be seen that the tidal mixing front is only present in summer (Fig. 4, bottom panel), when the water is stratified on the deeper flanks of the bank but not in the well-mixed crest area. The tidal mixing front may act as a barrier that limits the cross-frontal exchange of biological quantities (including nitrogen and plankton) between the central portion of the bank and surrounding deep areas (Chen and Beardsley, 2002).

3.2. Biological fields

In this section, selected results from the baseline model run are presented, including nitrogen and phytoplankton distributions in winter (March) and summer (August). The results represent unique distributional patterns of biological quantities under two significantly different biological and physical conditions. The modeled seasonal cycles of nitrogen and phytoplankton at fixed stations are presented in other sections, including data-model comparison (Section 3.3) and the comparison between baseline and BEC model runs (Section 3.5).

The 3-D biological fields begin to evolve after the model is started from the initial distribution on January 1, 1995. As an example, during March, the nutrient concentration remains high on GB (Fig. 5, top two

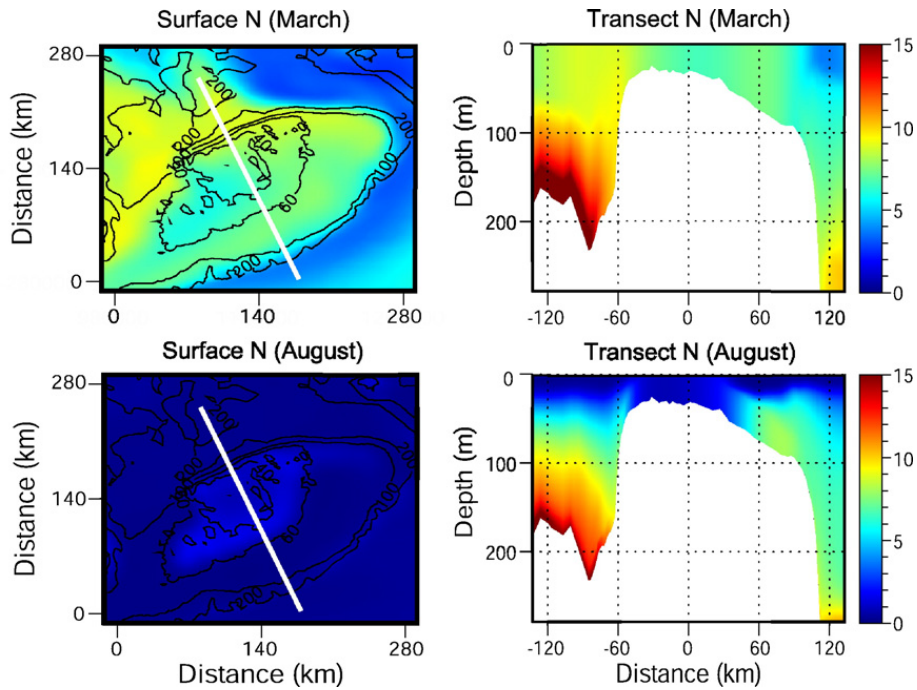


Fig. 5. Model distributions of nutrients (nitrogen, unit: $\mu\text{M N}$) at the surface and along the transect (white line) across the bank in March and August, 1995.

panels), with concentrations between 6 and 8 μM , except on the shallow crest of the bank where nutrients are lower due to increased uptake by the larger phytoplankton population there (Fig. 6, top two panels). Nutrient concentrations continue to drop from spring to summer

and reach low values ($< 1 \mu\text{M}$) on the crest of bank and in the surface layer of the deeper regions during summer (Fig. 5, bottom two panels). Near the tidal mixing front (40–60 m isobaths), a relatively higher nitrogen concentration ($> 1 \mu\text{M}$) persists throughout the summer, due to

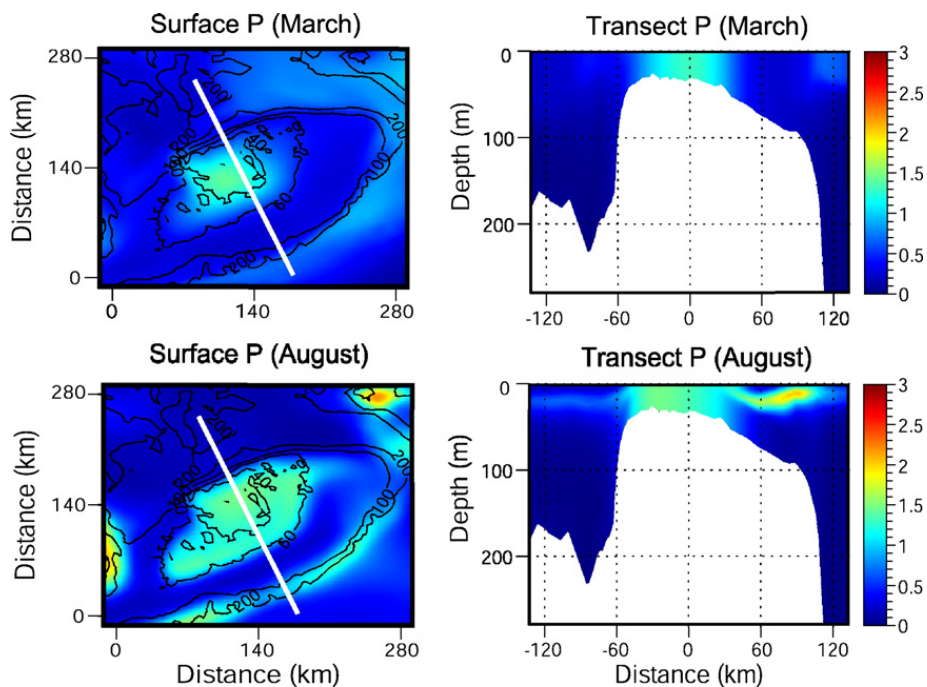


Fig. 6. Model distribution of phytoplankton (unit: $\mu\text{M N}$) at the surface and along the transect (white line) across the bank in March and August, 1995.

the tidal pumping process that brings up the deep nutrient-rich water onto the bank (Chen and Beardsley, 1998; Chen et al., 2003b; Hu et al., submitted for publication) and fuels high new production in that region (Horne et al., 1989; Franks and Chen, 1996; Townsend and Pettigrew, 1997; Townsend et al., 2006). Meanwhile, phytoplankton concentration during summer remains high inside the tidal mixing front (Fig. 6, bottom two panels), largely due to recycled production (a detailed analysis of the seasonal variation of new versus recycled nitrogen inside the 60-m isobath is described in Section 3.4).

The model also reveals that persistent subsurface phytoplankton maxima exist in the stratified deeper waters throughout the summer (see Fig. 6 bottom right panel for the example). Phytoplankton concentration at ~30 m below the surface is typically 3–5 times higher than the surface concentration, and can be one order of magnitude

higher in certain areas such as the southern flank. The subsurface phytoplankton maximum has been seen in many field surveys in the GoM (e.g. Holligan et al., 1984; Townsend et al., 2005), and its formation is mainly caused by the effect of nutrient and light availability near the pycnocline/nitracline, possibly in combination with the vertical movement of phytoplankton. Since no active vertical migration of phytoplankton (especially the dinoflagellates) is included in the model, some of the observed vertical distributional patterns, such as a bimodal distribution (chl-*a* maxima in both surface and subsurface layers) (Townsend et al., 2005), can not be reproduced. However, the general pattern of the phytoplankton vertical distributional has been captured reasonably well (see more comparisons in next section), indicating that the analysis of nitrogen and phytoplankton dynamics based on this model is a reasonable approximation.

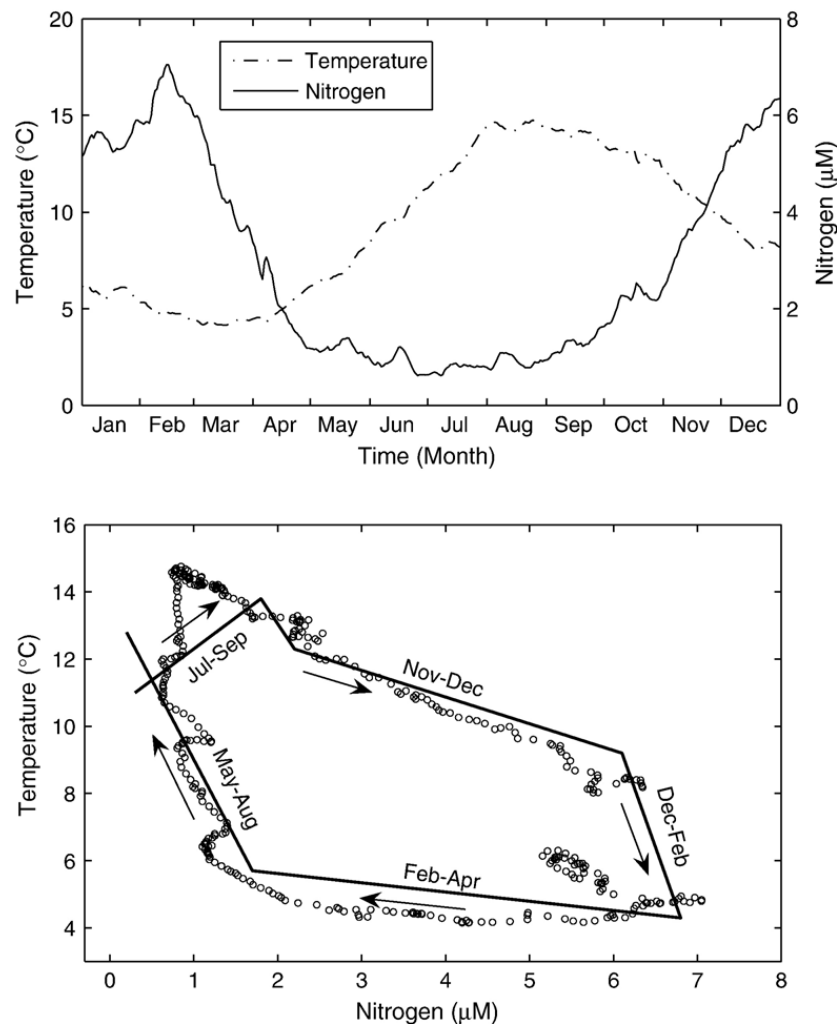


Fig. 7. Annual cycle of temperature versus nitrogen on Georges Bank (here nitrogen refers to dissolved inorganic nitrogen). Top panel: model-computed seasonal cycles of temperature and nitrogen. Bottom panel: comparison of model computed and observed nitrogen-temperature cycles. The solid polygon lines are plotted based on mean values of water samples collected in the shallow central part of the bank (<65 m) in 1975–1976 (adapted from Pastuszak et al., 1982, Fig. 3). Open circles represent model-computed temperature-nitrogen values on the crest of the bank.

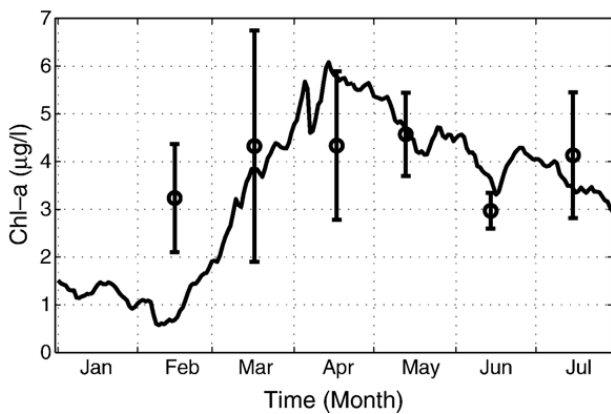


Fig. 8. Model-data comparison of chl-*a* concentrations on the central bank. The black line is the model time series at location A indicated in Fig. 1. The black circles with error bars (\pm standard deviation) are observed chl-*a* concentrations at three stations near location A (chl-*a* data converted from measurements by CTD-mounted fluorometers).

3.3. Model-data comparison

Pastuszak et al. (1982) examined the annual cycle of temperature versus nitrate on GB by measuring samples throughout the water column in the shallow central part of the bank (<65 m) during nine cruises between July 1975 and August 1976 (Fig. 7, black polygon lines at the bottom panel). Their results show that the concentration of nitrate reached a maximum in winter, accompanied by cooler temperature; and decreased to near zero in summer as the water warmed. The recharge and depletion of nitrate on the bank occurred on a short time scale (~ 2 months). This general pattern is reproduced in the 1995 model run as seen in the nitrogen-temperature plot (Fig. 7, top panel and open circles at the bottom panel), suggesting that the model captured the main seasonal nitrogen cycle reasonably well.

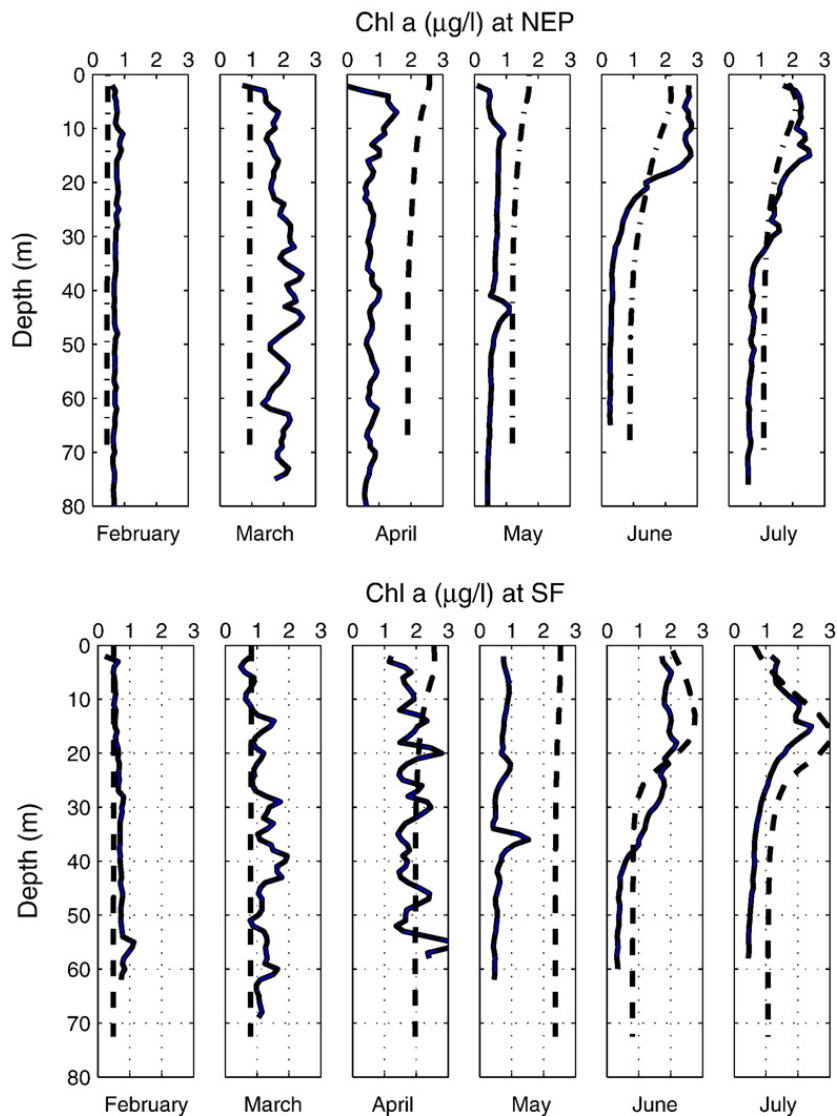


Fig. 9. Model-data comparison of chl-*a* concentrations (vertical profiles from February to July, 1995) on the Northeast Peak (NEP, location B in Fig. 1, top panel) and the southern flank (SF, location C in Fig. 1, bottom panel). The data shown in solid line, the model results in dashed line.

A limited amount of chl-*a* data is available to be compared with the modeled phytoplankton concentrations on GB. These data were collected using CTD-mounted fluorometers during the GLOBEC broad-scale surveys from January to July 1995, and were converted to chl-*a* concentration after calibration with water samples. The data-model comparison was conducted for three locations, including the center of the bank, the Northeast Peak, and the southern flank (shown as A, B, and C in Fig. 1), representing different physical locations and mixing regimes. The timing and magnitude of the spring phytoplankton blooms and sustained high chl-*a* concentrations ($>3 \mu\text{g l}^{-1}$) throughout the early summer in the well-mixed region have been captured by the model reasonably well (Fig. 8), except in February when the modeled value is lower than the observed mean. This comparison needs to be viewed with caution due to the large range of the data values in certain months (e.g. March; Fig. 8) resulting from the high degree of phytoplankton patchiness (especially during the spring bloom period). Observed phytoplankton concentrations vary significantly even in nearby stations that have similar bottom depths and mixing regimes. However, this kind of small-scale patchiness is unlikely to be reproduced in this model largely due to the limit on the spatial resolution of model grid, bottom topographic, and surface forcing information.

The vertical profiles of chl-*a* are also compared between data and model on the Northeast Peak (Fig. 9 top panels) and the southern flank (Fig. 9 bottom panels), where the water columns were well-mixed from January to April and became stratified after May. The phytoplankton concentration remained low throughout the water column before April in both the field data and model results, and increased in the surface layer after May as water became stratified. Characteristic patterns in the observed vertical distribution, such as the subsurface chl-*a* maxima in July on the southern flank, also have been reproduced in the model.

3.4. Nitrogen flux

Nitrogen dynamics associated with both physical transport and biological source/sink terms were examined here. The physical transport refers to the transport of dissolved inorganic nitrogen (DIN), whereas the source and sink terms refer to the production of DIN through internal recycling and the uptake of DIN through photosynthesis, respectively.

The physical transport of nutrients across the 60-m isobath (i.e., the net flux of N) onto the central bank varied significantly throughout the year (Fig. 10, top panel, with

an annually averaged flux of $262.23 \text{ mol N s}^{-1}$. The flux between late spring and late fall (April–November) is relatively low with an average value of $225.47 \text{ mol N s}^{-1}$; while the average flux in later winter and early spring is about 70 mol N s^{-1} higher than the annually averaged value mainly due to episodic high-flux events during winter time, which appear to be associated with strong storms passing by the bank that might contribute to the elevated average flux and a quick recharge of nitrogen on the bank. On the other hand, during the late spring and fall, relatively lower nitrogen fluxes are expected as the result of the formation of the tidal mixing front near the 60-m isobath and the depletion of surface nitrogen in the surrounding waters. During this period, a large gradient develops between the crest and surrounding waters in water-column averaged nutrient concentration due to

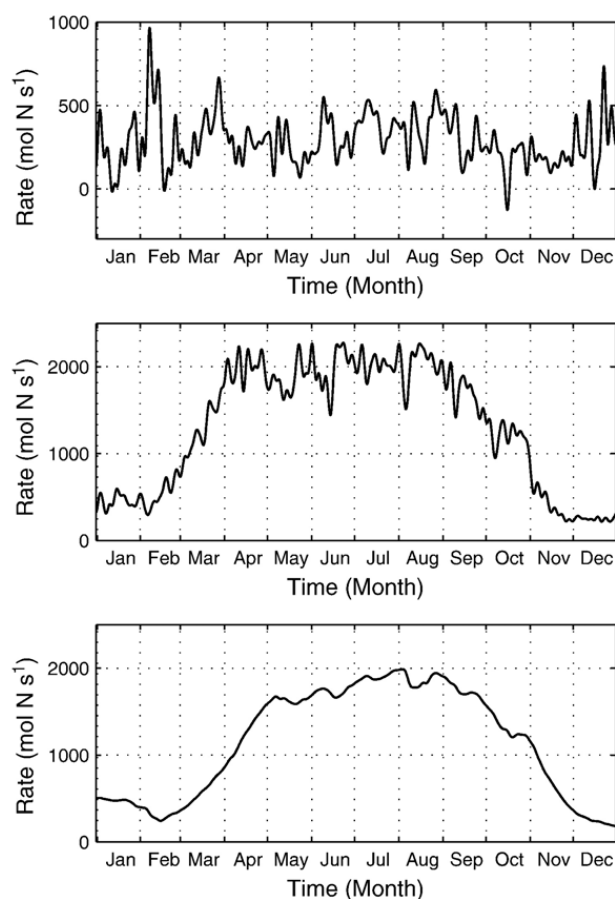


Fig. 10. Model-computed variation of physical transport of dissolved inorganic nitrogen across the 60-m isobath (i.e., net flux of N) into the crest area (top panel), internal biological sink (N uptake by P) (middle panel), and source (recycled N) (bottom panel) integrated over the entire water body inside the 60 m isobath on Georges Bank for 1995. The fluxes were computed from 2-minute model output (every time step) to obtain hourly averaged time-series and then low-pass filtered using PL66 filter (Flagg et al., 1976) which has a half-power point at 33 hours. This filtering removes tidal and higher-frequency fluctuations from the time-series data.

uptake by the large crest phytoplankton population (Fig. 5). The model reveals that although such a gradient would tend to increase the on-crest flux of nutrients, the cross-isobath exchange (volume transport) is reduced during this warmer period by the tidal mixing front. The estimation of cross-frontal nutrient transport based on our model results is significantly lower than previous estimates and will be discussed in detail in the following paragraphs.

The internal biological sink (Fig. 10, middle panel) and source (Fig. 10, bottom panel) terms of dissolved inorganic nitrogen were computed by integrating these two terms over the entire water body inside the 60-m isobath on GB. The source term represents nutrient recycling from the remineralization of detritus and the excretion of zooplankton and top predators; while the sink term represents the loss of nutrients through uptake by phytoplankton. The peak nutrient sink occurred in the beginning of April (Fig. 10, middle panel) when phytoplankton uptake of nutrients (i.e. gross primary productivity) reaches its maximum. This peak is simply a result of increasing surface irradiance and sufficient nutrient supply as well as the increase of phytoplankton standing stock during this time of the year. Likewise the nutrient sink increased due to the increase of internal nutrient recycling and reached a peak value of $1.28 \times 10^3 \text{ mol N s}^{-1}$ in April (Fig. 10, bottom panel). This increase is largely due to the increase of the detritus pool and the rise in water temperature during spring. The model results suggest that the contribution of internal recycling to the nitrogen supply is significantly greater than the physical transport during most of the year (from April to November). The ratio of internal recycling versus physical transport varies from 4 to 5 during the summer months (June–August), which corresponds to an f ratio (ratio of production based on new nutrients supplied from outside of the bank to total production) of ~ 0.17 to 0.2 on the central bank. This value agrees well with the f ratios of 0.1–0.2 measured using ^{15}N uptake techniques by Harrison et al. (1990) and Loder et al. (1992), but somewhat lower than the estimate (0.23–0.31) by Horne et al. (1989) using similar techniques. The general pattern of the observed highly-recycled production on the central bank is well captured by this model.

The strong internal nitrogen recycling allows for high primary productivity on the central bank even during the summer months when the nitrogen concentration is very low. Using the ^{14}C uptake technique, O'Reilly et al. (1987) estimated that the primary productivity on the central bank is about $1\text{--}2 \text{ gC m}^{-2} \text{ day}^{-1}$ during most of the year, including the summer months. Our model results

indicate that the average summertime (June–August) productivity (sink term in Fig. 3) is $1.47 \times 10^3 \text{ mol N s}^{-1}$ for the total area inside the 60-m isobath (this area is $1.396 \times 10^4 \text{ km}^2$), which is equivalent to $9.1 \times 10^{-3} \text{ } \mu\text{mol N m}^{-2} \text{ day}^{-1}$, or $0.72 \text{ gC m}^{-2} \text{ day}^{-1}$ if the Redfield ratio (C:N=6.6 in phytoplankton cells) is used to convert between nitrogen and carbon assimilation rates. This value appears to be below the range of $1\text{--}2 \text{ gC m}^{-2} \text{ day}^{-1}$ estimated by O'Reilly et al. (1987). However, this result must be considered with caution, since the use of the Redfield ratio might not be appropriate in this case. First, the assimilation and composition ratios can be equal only when the steady state is reached. A much higher assimilation ratio (>10.0) is often observed in nitrate-depleted surface waters (e.g. Eppley et al., 1979). In fact, the assimilation ratio can be as high as 15 based on the concurrent measurements of carbon and nitrogen assimilation rates on the central GB (Table 1 in Horne et al., 1989). Second, the C:N composition ratio of phytoplankton can also be 2–3 times higher than the Redfield ratio in a nitrogen-depleted condition (Parsons et al., 1961; Banse, 1974; Goldman et al., 1979), suggesting that phytoplankton might increase the C:N assimilation ratio in order to maintain a high observed C:N composition ratio. Overall, it is very likely that the model-computed primary productivity falls in the observed $1\text{--}2 \text{ gC m}^{-2}$ range given that the C:N assimilation rate can reach 10–15 on the bank.

Horne et al. (1989) showed that the measured cross-frontal (horizontal) flux of nitrate ($\sim 5 \times 10^3 \text{ mol N s}^{-1}$) was more than adequate to meet the nitrogen requirements of the frontal zone and mixed area in a depth-integrated sense. They argued that this cross-frontal flux may not be caused by a so-called shear-flow dispersion mechanism, by which nutrient-rich subsurface water parcels periodically moving onto the bank with the tidal flow and return half a tidal period later with their nutrient concentration reduced as a result of vertical mixing. Rather, the large eddy fluxes observed on GB in 1978 and in 1985 appear to be largely caused by interactions of a rotary velocity field with the vertical nitrate gradient, a mechanism termed “skew flux” (Loder and Horne, 1991).

Townsend and Pettigrew (1997) employed a different method to compute the cross-frontal nitrogen fluxes, using the nitrogen gradients observed across the 60-m isobath in May 1993 and a model-derived horizontal dispersion coefficient of $250 \text{ m}^{-2} \text{ s}^{-1}$ (Loder et al., 1982). They estimated the total flux into the vertically well-mixed region of the bank inside the 60-m isobath to be $\sim 480 \text{ mol N s}^{-1}$, a value close to the estimate by Garrett and Loder (1981) and Loder and Platt (1985),

but significantly (about 10-fold) lower than that estimated by Horne et al. (1989). Townsend and Pettigrew (1997) argued that Horne et al. (1989) might have over-estimated the cross-frontal nitrogen flux due to the under-resolved moored measurements upon which they based their advection and eddy flux estimation, and that nitrate fluxes into the well-mixed region of GB may only support 12–24% of the total estimated primary production. The flux computed from our model supports Townsend and Pettigrew's (1997) argument, suggesting that the cross-frontal exchange is much smaller than the total nitrogen demand by phytoplankton on the central bank.

To identify which physical mechanisms are responsible for the cross-frontal exchange, a recent study by Ullman et al. (2003) computed buoyancy fluxes across the tidal mixing front on the northern flank of GB in spring using concurrent CTD and ADCP velocity measurements over a 12-day period. They found that the observed tidal-pumping flux, arising from the covariance between buoyancy and velocity phase means, is predominantly due to the cross-isobath component of the skew flux computed using a diagnosed tidal vertical velocity field and mean buoyancy gradients. Although this flux calculation supports the skew flux hypothesis by Horne et al. (1989), Ullman et al. (2003) computed only buoyancy fluxes induced by vertical salinity gradients in spring; whereas the difference in the vertical profiles of salinity and nutrients can affect the results of skew flux calculation significantly.

3.5. Possible effects of NAO on GB nitrogen and phytoplankton dynamics

It has been recognized that the properties of the Slope Water entering the GoM/GB system at depth can be influenced by large-scale external forcings, such as the North Atlantic Oscillation (NAO) (Petrie and Drinkwater, 1993; Drinkwater and Gilbert, 2004). During low NAO years, the Labrador Slope Water (LSW) from the north can extend further southwestward along the slope and enter the GoM through the Northeast Channel (NEC). The LSW is colder, fresher and about 50% lower in dissolved inorganic nitrogen (Thomas et al., 2003; Townsend et al., 2006) than the Warm Slope Water (WSW), the dominant water mass entering the GoM following high or regular NAO years. The linkage between NAO lows and LSW influx into the GoM has been observed in the 1960's, manifested by the lower bottom water temperature throughout the GoM during that time period (Petrie and Drinkwater, 1993). This linkage occurs again as a significant amount of LSW

entered the GoM during 1998 in response to the very low NAO condition in 1996, with a time lag of about two years (Pershing et al., 2001).

One interesting question is whether the NAO-dependent change of nutrient concentration in this deep Slope Water can influence the nitrogen dynamics and primary production processes on GB. A conceptual model formed by Townsend et al. (2006) has suggested that a possible direct link may exist, given that the tidal pumping process (Chen and Beardsley, 1998) can bring the nutrient-rich deep Slope Water onto the bank. Specifically, the northern flank of the bank is the key area where the cross-frontal mixing and nutrient injections onto the bank occurs more significantly than the other parts of the bank (Pastuszak et al., 1982; Townsend and Pettigrew, 1997; Houghton and Ho, 2001). This may lead to greater phytoplankton biomass accumulation near the Northeast Peak (Cura et al., 1987), where the “jet” current on the northern flank spreads out, possibly enhancing the tidal pumping in that region. This conceptual model illustrates nicely the pathway of the nutrient transport and its biological consequences regarding the enhancement of new production on the northeast peak and along the tidal mixing front on the northern and southern flanks. Yet a more rigorous test of this conceptual model is necessary in order to establish a direct link between NAO and productivity on the bank.

Our numerical model proved to be a useful tool for examining the above conceptual model quantitatively. In this study, we focus on the specific question of whether the change in nutrient concentration in the Slope Water can affect the nutrient flux into the well-mixed central bank (inside the 60-m isobath) and thereby change the primary productivity. This question involves both biological and physical processes and is difficult to address by examining individual processes separately. For instance, much of the nutrient flux on the northern edge of the bank can also be utilized by phytoplankton before dispersing across the top of the bank (Townsend et al., 2006), which might weaken the role played by the tidal pumping process. In fact, the model comparison between the baseline and BEC cases suggests that, with nutrient concentration 50% higher in the BEC case, the total nutrient transport across the 60-m isobath increased about 12% during winter/spring months, and only 5% during summer months (Fig. 11a). The total nutrient uptake (equivalent to total primary productivity) also only shows slight increases in the BEC case, with a higher increase during the summer months than during winter/spring (3.6% versus 1.8% as shown in Fig. 11a). Thus, the concentrations of nutrients

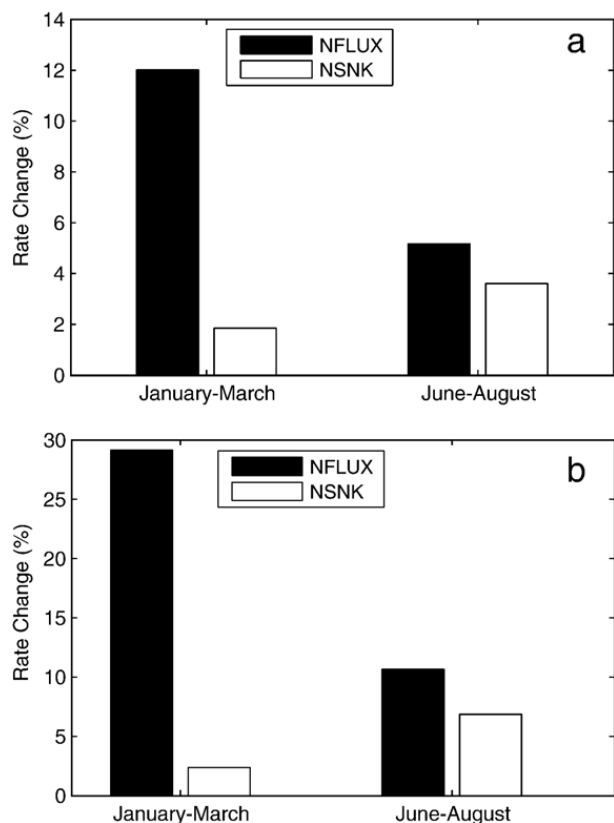


Fig. 11. Model-computed differences between baseline and bottom enriched condition (BEC) cases of 1) physical transport of nutrients across the 60-m isobath (NFLUX, black bars) and 2) internal biological sink (NSNK, white bars) integrated over the entire water body inside the 60-m isobath on Georges Bank in winter/spring and summer months. Top panel (a) is for a domain inside the 60 m isobath while bottom panel (b) is for a domain inside the 100 m isobath. The difference is expressed as a percentage change, $100 * (\text{BEC} - \text{baseline}) / \text{baseline}$.

and phytoplankton inside the well-mixed area increase slightly in response to the change of nutrient concentration in the deep Slope Water (Fig. 12). The difference in phytoplankton concentration between the two cases is lower than 3% during December–March, likely due to the fact that phytoplankton photosynthesis is more limited by PAR than nutrients during that time period (Ji et al., 2006b). In addition, the relatively small difference during summer and fall (<7.5%) is also understandable, since the new production supported by nutrient supply through physical transport contributes only ~1/5 of the total production on the central bank (due to weak cross-frontal exchange).

When the domain used for flux calculation was extended to include the entire area inside the 100 m isobath of the bank, our simulation results suggest that the increase of nitrogen concentration may have a relatively more significant impact on the nitrogen transport and primary production (than for the 60 m isobath case). The

comparison of the BEC and baseline cases indicates that the total nutrient transport across the 100 m isobath increased 29% during winter/spring months, and 11% during summer months (Fig. 11b). As a result, the total primary productivity inside the 100 m isobath increased by 2% and 7.5% respectively. Ecologically, such increases (especially during summer months) may have more important consequences, since many higher trophic level production processes occur in the deeper flank region between 60 m and 100 m isobaths (Meise and O'Reilly, 1996; Lough and Manning, 2001).

One caveat of the above simple numerical experiment is that no NAO-induced change in physical properties of the water mass was incorporated in the model. Since significant differences exist between LSW and WSW regarding their temperature and salinity structures, the stratification and stability of the water column are expected to be different accordingly. Such differences will inevitably change the mixing processes and consequently the nitrogen transport. Moreover, since WSW is warmer, more saline and nutrient rich than LSW, it enhances the upward doming of isopycnal surfaces which may isolate an upper mixed layer, promoting phytoplankton blooms in the GoM (Townsend and Spinard, 1986). As a result, a series of nonlinear responses of the biological system across the GoM/GB region might be triggered. In addition, a more vigorous validation on the model simulation of vertical processes is needed, since the on-bank transport of bottom nutrient-rich water could be sensitive to the dynamics of vertical mixing and advection processes. Nevertheless, the simplification in our numerical experiment allows us to

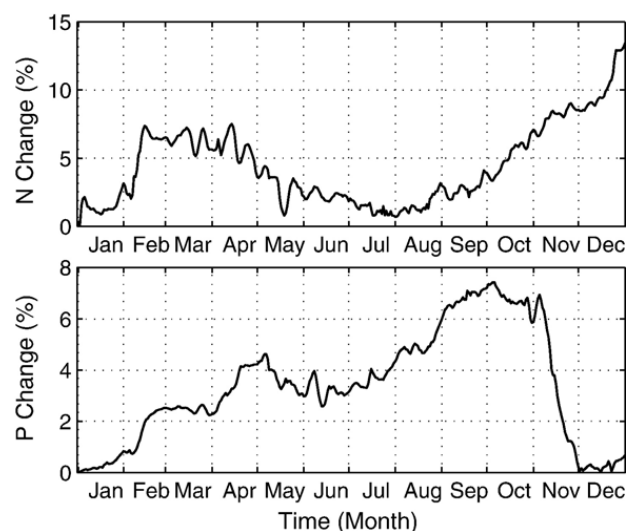


Fig. 12. Model-computed percent change of nutrient (top panel) and phytoplankton (bottom panel) concentrations on the central bank (location A in Fig. 1) throughout 1995.

focus on the system response to the change of nutrient concentration only, such that it provide a first-order assessment of potential influence of NAO on the nutrient cycle and primary productivity on GB, with an initial conclusion that an NAO-dependent change of nutrient concentration in the deep Slope Water entering the GoM system may have little impact on the interannual variability of nutrient and phytoplankton dynamics in the well-mixed part of GB, but have relatively more significant impact in the deep flank areas.

4. Conclusions

The biological–physical coupled model for the GoM/GB region presented here provides a valuable tool for examining the influences of local and external processes on the nutrient and phytoplankton dynamics on GB. The model captured the general pattern of spatial-temporal distributions of nutrient and phytoplankton concentrations on GB and provided a more quantitative estimation of nutrient flux by integrating the transport over a longer time period and a complete spatial domain. The results suggest that:

- (1) Between late spring and fall, the nutrient sources that support primary production on the central GB are mainly through internal nutrient recycling, while the major nutrient recharge from outside of the bank occurs during winter.
- (2) During the summer months, nutrient supply through physical transport (e.g. tidal pumping) contributes about 1/5 of the total nutrient demand, with an estimated transport at least 50% less than previous estimations.
- (3) The comparison of model runs with different nutrient concentrations in the deep GoM water suggests that these potential NAO-induced changes in deep nutrient concentration may have little impact on nutrient and phytoplankton dynamics in the well-mixed central area of GB, but have relatively more significant impact in the deep flank areas.

Acknowledgements

This research was supported by the US GLOBEC/GB IV-B Program through NOAA grant NA-17RJ1223 to RJ, CSD and RCB; NSF OCE-0606928 to CC; NSF OCE-0727033 to RJ; and Smith Chair in Coastal Oceanography to RCB. We would like to thank Q. Xu for his help on setting up the physical model run; R. Tian for providing initial biological conditions (with original

data from Pierre Clement at Bedford Institute of Oceanography); G. Cowles for his help on FVCOM parallel run and post-processing; and S. Hu for providing MM5 model output. Dr. E. Durbin (University of Rhode Island) provided the fluorescence-converted Chl-*a* data. Discussion with Dr. D. Townsend (University of Maine) on the nutrient and phytoplankton dynamics on GB has been very helpful. Two anonymous reviewers made suggestions which helped improve the manuscript. The US GLOBEC contribution number is 543.

References

- Anderson, T.R., 2005. Plankton functional type modelling: running before we can walk? *Journal of Plankton Research* 27 (11), 1073–1081.
- Anderson, T.R., 2006. Confronting complexity: reply to Le Quéué and Flynn. *Journal of Plankton Research* 28 (9), 877–878.
- Banse, K., 1974. On the interpretation of data from the nitrogen to carbon ratio in phytoplankton. *Limnology and Oceanography* 19, 695–699.
- Brink, K.H., 2004. The grass is greener in the coastal ocean: coastal waters teem with life, but sometimes scientist can't explain why. *Oceanus* 42 (3), 1–3.
- Butman, B., et al., 1982. Recent observations of the mean circulation on Georges Bank. *Journal of Physical Oceanography* 12, 569–591.
- Chen, C., Beardsley, R., 1998. Tidal mixing and cross-frontal particle exchange over a finite amplitude asymmetric bank: a model study with application to Georges Bank. *Journal of Marine Research* 56, 1163–1201.
- Chen, C., Beardsley, R., 2002. Cross-frontal water exchange on Georges Bank: modeling exploration of the US GLOBEC/Georges Bank phase III study. *Journal of Oceanography* 58, 403–420.
- Chen, C., Beardsley, R.C., Limeburner, R., 1995. Numerical study of stratified tidal rectification over finite-amplitude banks. Part II: Georges Bank. *Journal of Physical Oceanography* 25, 2111–2128.
- Chen, C., Beardsley, R., Franks, P.J.S., 2001. A 3-D prognostic numerical model study of the Georges Bank ecosystem. Part I: physical model. *Deep-Sea Research. Part 2. Topical Studies in Oceanography* 48 (1–3), 419–456.
- Chen, C., Liu, H., Beardsley, R.C., 2003a. An unstructured, finite-volume, three-dimensional, primitive equation oceanography model: application to coastal oceanography and estuaries. *Journal of Atmospheric and Oceanic Technology* 20, 159–186.
- Chen, C., Xu, Q., Beardsley, R.C., Franks, P.J.S., 2003b. Model study of the cross-frontal water exchange on Georges Bank: a three-dimensional Lagrangian experiment. *Journal of Geophysical Research* 108 (C5), 3142. doi:10.1029/2000JC00390.
- Chen, C., Beardsley, R., Hu, S., Xu, Q., Liu, H., 2005. Using MM5 to hindcast the ocean surface forcing fields over the Gulf of Maine and Georges Bank region. *Journal of Atmospheric and Oceanic Technology* 22 (2), 131–145.
- Chen, C., Beardsley, R.C., Cowles, G., 2006a. An unstructured grid, finite-volume coastal ocean model (FVCOM) system. Special Issue entitled “Advance in Computational Oceanography”. *Oceanography* 19 (1), 78–89.
- Chen, C., Beardsley, R.C., Xu, Q., Limeburner, R., 2006b. Tidal dynamics in the Gulf of Maine and New England Shelf: an application of FVCOM. *Deep-Sea Research. Part 2. Topical Studies in Oceanography* (in revision).

- Chen, C., Cowles, G., Beardsley, R.C., 2006c. An Unstructured Grid, Finite-volume Coastal Ocean Model: FVCOM User Manual, Second edition.
- Chen, C., et al., 2007. A finite volume numerical approach for coastal ocean circulation studies: comparisons with finite difference models. *Journal of Geophysical Research* 112, C03018. doi:10.1029/2006JC003485.
- Cowles, G., Lentz, S., Chen, C., Xu, Q., Beardsley, R., submitted for publication. Comparison of observed and model-computed low frequency circulation and hydrography on the New England shelf. *Journal of Geophysical Research*.
- Cura, J.J., Backus, R.H., Bourne, D.W., 1987. Phytoplankton, Georges Bank. MIT Press, Cambridge, Massachusetts, pp. 213–218.
- Drinkwater, K.F., Gilbert, D., 2004. Hydrographic variability in the waters of the Gulf of St. Lawrence, the Scotian Shelf and the eastern Gulf of Maine (NAFO Subarea 4) during 1991–2000. *Journal of Northwest Atlantic Fishery Science* 34, 83–99.
- Dudhia, J., et al., 2003. PSU/NCAR Mesoscale Modeling System Tutorial Class Notes and User's Guide, MM5 Modeling System version 3, Mesoscale and Microscale Meteorology Division. National Center for Atmospheric Research.
- Edwards, A.M., 2001. Adding detritus to a nutrient–phytoplankton–zooplankton model: a dynamical-systems approach. *Journal of Plankton Research* 23 (4), 389–413.
- Eppley, R.W., Renger, E.H., Harrison, W.G., 1979. Nitrate and phytoplankton production in southern California coastal waters. *Limnology and Oceanography* 24 (3), 483–494.
- Flagg, C.N., Vermersch, J.A., Beardsley, R., 1976. New England shelf dynamics experiment (March 1974) data report — part II: the moored array. Dept. Meteor. M.I.T. GFD Lab. Rep., vol. 75-1.
- Flagg, C.N., Backus, R.H., Bourne, D.W., 1987. Hydrographic Structure and Variability, Georges Bank. MIT Press, Cambridge, Massachusetts, pp. 108–124.
- Franks, P.J.S., 2002. NPZ models of plankton dynamics: their construction, coupling to physics, and application. *Journal of Oceanography* 58 (379–387).
- Franks, P.J.S., Chen, C.S., 1996. Plankton production in tidal fronts: a model of Georges Bank in summer. *Journal of Marine Research* 54 (4), 631–651.
- Franks, P.J.S., Wroblewski, J.S., Flierl, G.R., 1986. Behavior of a simple plankton model with food-level acclimation by herbivores. *Marine Biology* 91, 121–129.
- Friedrichs, M.A.M., Hofmann, E.E., 2001. Physical control of biological processes in the central equatorial Pacific Ocean. *Deep-Sea Research. Part 1. Oceanographic Research Papers* 48, 1023–1069.
- Friedrichs, M.A.M., Hood, R.R., Wiggert, J.D., 2006. Ecosystem model complexity versus physical forcing: quantification of their relative impact with assimilated Arabian Sea data. *Deep-Sea Research. Part 2. Topical Studies in Oceanography* 53, 576–600.
- Galperin, B., Kantha, L.H., Hassid, S., Rosati, A., 1988. A quasi-equilibrium turbulent energy model for geophysical flows. *Journal of the Atmospheric Sciences* 45, 55–62.
- Garrett, C.J.R., Loder, J.W., 1981. Dynamical aspects of shallow sea fronts. *Philosophical Transactions of the Royal Society of London A302*, 563–581.
- GLOBEC, 1992. Northwest Atlantic Implementation Plan. U.S. Global Ocean Ecosystem Dynamics Report, vol. 6.
- Goldman, J.C., McCarthy, J.J., Peavey, D.G., 1979. Growth rate influence on the chemical composition of phytoplankton in oceanic waters. *Nature* 279 (5710), 210–215.
- Harrison, W.G., Horne, E.P.W., Irwin, B., Platt, T., 1990. Biological production on Georges Bank: are tidal fronts primary sources of new production in summer? *Eos, Transactions of the American Geophysical Union* 71, 96.
- Holligan, P.M., Balch, W.M., Yentsch, C.M., 1984. The significance of subsurface chlorophyll, nitrite and ammonium maxima in relation to nitrogen for phytoplankton growth in stratified waters of the Gulf of Maine. *Journal of Marine Research* 42, 1051–1073.
- Horne, E.P.W., et al., 1989. Nitrate supply and demand at the Georges Bank tidal front. *Scientia Marina* 53 (2–3), 145–158.
- Horne, E.P.W., Loder, J.W., Naimie, C.E., Oakey, N.S., 1996. Turbulence dissipation rates and nitrate supply in the upper water column on Georges Bank. *Deep-Sea Research. Part 2. Topical Studies in Oceanography* 43 (7–8), 1683–1712.
- Houghton, R.W., Ho, C., 2001. Diapycnal flow through the Georges Bank tidal front: a dye tracer study. *Geophysical Research Letter* 28 (1), 33–36.
- Hu, S., Townsend, D., Chen, C., Beardsley, R., Cowles, G., submitted for publication. Tidal pumping-induced nutrient refreshment on Georges Bank: A process modeling experiment. *Journal of Geophysical Research*.
- Ji, R., et al., 2006a. The impact of Scotian Shelf Water “cross-over” on the plankton dynamics on Georges Bank: a 3-D experiment for the 1999 spring bloom. *Deep-Sea Research. Part 2. Topical Studies in Oceanography* 53 (23–24), 2684–2707.
- Ji, R., et al., 2006b. Spring bloom and associated lower trophic level food web dynamics on Georges Bank: 1-D and 2-D model studies. *Deep-Sea Research. Part 2. Topical Studies in Oceanography* 53 (23–24), 2656–2683.
- Ji, R., et al., 2006c. Cross-frontal exchange of *Calanus finmarchicus* on Georges Bank: a study using in-situ data from Video Plankton Recorder (VPR) surveys and a dye release experiment and a Lagrangian model. *Eos, Transactions of the American Geophysical Union* 87 (36) (Ocean Sci. Meet. Suppl., Abstract OS33H-04).
- Klein, P., Backus, R.H., Bourne, D.W., 1987. A simulation of some physical and biological interactions, Georges Bank. MIT Press, Cambridge, Massachusetts, pp. 395–402.
- Limeburner, R., Beardsley, R., 1996. Near-surface recirculation over Georges Bank. *Deep-Sea Research. Part 2. Topical Studies in Oceanography* 43 (7–8), 1547–1574.
- Loder, J.W., 1980. Topographic rectification of tidal currents on the sides of Georges Bank. *Journal of Physical Oceanography* 10, 1399–1416.
- Loder, J.W., Horne, E.P.W., 1991. Skew eddy fluxes as signatures of non-linear tidal current interactions, with application to Georges Bank. *Atmosphere-Ocean. Toronto ON* 29 (3), 517–546.
- Loder, J.W., Platt, T., 1985. Physical controls on phytoplankton production at tidal fronts. In: Gibbs, P.E. (Ed.), *Proceedings of the Nineteenth European Marine Biology Symposium*. Cambridge University Press, pp. 3–21.
- Loder, J.W., Wright, D.G., Garrett, C., Juszko, B.A., 1982. Horizontal exchange on central Georges Bank. *Canadian Journal of Fisheries and Aquatic Sciences* 39, 1130–1137.
- Loder, J.W., et al., 1992. *Physics and Biology of the Georges Bank Frontal System*. Department of Fisheries and Oceans, Canada.
- Lough, R.G., Manning, J.P., 2001. Tidal-front entrainment and retention of fish larvae on the southern flank of Georges Bank. *Deep-Sea Research. Part 2. Topical Studies in Oceanography* 48, 631–644.
- Meise, C., O'Reilly, J.E., 1996. Spatial and seasonal patterns in abundance and age-composition of *Calanus finmarchicus* in the Gulf of Maine and on Georges Bank: 1977–1987. *Deep-Sea Research. Part 2. Topical Studies in Oceanography* 43, 1473–1501.

- Mellor, G.L., Yamada, T., 1982. Development of a turbulence closure model for geophysical fluid problems. *Reviews of Geophysics and Space Physics* 20, 851–875.
- Olascoaga, M.J., Idrisi, N., Romanou, A., 2005. Biophysical isopycnic-coordinate modelling of plankton dynamics in the Arabian Sea. *Ocean Modelling* 8, 55–80.
- O'Reilly, J.E., Evans-Zetlin, C.E., Busch, D.A., Backus, R.H., Bourne, D.W., 1987. *Primary Production, Georges Bank*. MIT Press, Cambridge, Massachusetts, pp. 220–233.
- Parsons, T.R., Stephens, K., Strickland, J.D.H., 1961. On the chemical composition of eleven species of marine phytoplankters. *Journal of the Fisheries Research Board of Canada* 18, 1001–1016.
- Pastuszek, M., Wright, W.R., Patanjo, D., 1982. One year of nutrient distribution in the Georges Bank region in relation to hydrography, 1975–1976. *Journal of Marine Research* 40, 525–542.
- Pershing, A.J., et al., 2001. Oceanographic response to climate in the Northwest Atlantic. *Oceanography* 14, 76–82.
- Petrie, B., Drinkwater, K.F., 1993. Temperature and salinity variability on the Scotian Shelf and in the Gulf of Maine 1945–1990. *Journal of Geophysical Research* 98 (11), 20079–20090.
- Popova, E.E., Fasham, M.J.R., Osipov, A.V., Ryabchenko, V.A., 1997. Chaotic behaviour of an ocean ecosystem model under seasonal external forcing. *Journal of Plankton Research* 19 (10), 1495–1515.
- Smagorinsky, J., 1963. General circulation experiments with the primitive equations, I. the basic experiment. *Monthly Weather Review* 91, 99–164.
- Steele, J.H., Henderson, E.W., 1992. The role of predation in plankton models. *Journal of Plankton Research* 14, 157–172.
- Thomas, A.C., Townsend, D.W., Weatherbee, R., 2003. Satellite-measured phytoplankton variability in the Gulf of Maine. *Continental Shelf Research* 23, 971–989.
- Townsend, D.W., Pettigrew, N.R., 1997. Nitrogen limitation of secondary production on Georges Bank. *Journal of Plankton Research* 19 (2), 221–235.
- Townsend, D.W., Spinard, R.W., 1986. Early phytoplankton blooms in the Gulf of Maine. *Continental Shelf Research* 6, 515–529.
- Townsend, D.W., Thomas, A.C., 2001. Winter-spring transition of phytoplankton chlorophyll and inorganic nutrients on Georges Bank. *Deep-Sea Research. Part 2. Topical Studies in Oceanography* 48 (1–3), 199–214.
- Townsend, D.W., Thomas, M., 2002. Springtime nutrient and phytoplankton dynamics on Georges Bank. *Marine Ecology. Progress Series* 228, 57–74.
- Townsend, D.W., Bennett, S.L., Thomas, M.A., 2005. Diel vertical distributions of the red tide dinoflagellate *Alexandrium fundyense* in the Gulf of Maine. *Deep-Sea Research. Part 2. Topical Studies in Oceanography* 52 (19–21), 2593–2602.
- Townsend, D.W., Thomas, A.C., Mayer, L.M., Thomas, M., Quinlan, J., 2006. Oceanography of the Northwest Atlantic Continental Shelf. In: Robinson, A.R., Brink, K.H. (Eds.), *The Sea*, vol. 14. Harvard University Press, Cambridge, pp. 119–168.
- Ullman, D.S., Dale, A.C., Hebert, D., Barth, J.A., 2003. The front on the Northern Flank of Georges Bank in spring: 2. Cross-frontal fluxes and mixing. *Journal of Geophysical Research-Oceans* 108 (C11).
- Vitousek, P.M., Howarth, R.W., 1991. Nitrogen limitation on the land and in the sea: how can it occur? *Biogeochemistry* 13 (2), 87–115.
- Walsh, J.J., et al., 1987. Nitrogen Cycling on Georges Bank and the New York shelf: A Comparison Between Well-mixed and Seasonally Stratified Waters, Georges Bank. MIT Press, Cambridge, Massachusetts, pp. 234–246.
- Wiebe, P., Beardsley, R., Mountain, D., Bucklin, A., 2002. U.S. GLOBEC Northwest Atlantic/Georges Bank Program. *Oceanography* 15 (2), 13–29.